On the toroidal plasma rotations induced by lower hybrid waves

Xiaoyin Guan,[1] Hong Qin,[1,2] Jian Liu,[2] and Nathaniel J. Fisch[1]
[1]*Plasma Physics Laboratory, Princeton University, Princeton, New Jersey 08543, USA*
[2]*Department of Modern Physics, University of Science and Technology of China, Hefei, Anhui 230026, China*

(Received 13 November 2012; accepted 24 January 2013; published online 13 February 2013)

A theoretical model is developed to explain the plasma rotations induced by lower hybrid waves in Alcator C-Mod. In this model, torodial rotations are driven by the Lorentz force on the bulk-electron flow across flux surfaces, which is a response of the plasma to the resonant-electron flow across flux surfaces induced by the lower hybrid waves. The flow across flux surfaces of the resonant electrons and the bulk electrons are coupled through the radial electric field initiated by the resonant electrons, and the friction between ions and electrons transfers the toroidal momentum to ions from electrons. An improved quasilinear theory with gyrophase dependent distribution function is developed to calculate the perpendicular resonant-electron flow. Toroidal rotations are determined using a set of fluid equations for bulk electrons and ions, which are solved numerically by a finite-difference method. Numerical results agree well with the experimental observations in terms of flow profile and amplitude. The model explains the strong correlation between torodial flow and internal inductance observed experimentally, and predicts both counter-current and co-current flows, depending on the perpendicular wave vectors of the lower hybrid waves. © *2013 American Institute of Physics*. [http://dx.doi.org/10.1063/1.4791666]

I. INTRODUCTION

Plasma in tokamaks with rotation has many advantages. Strong rotation can stabilize magneto-hydrodynamic (MHD) instabilities[1,2] and gradients of plasma rotation help improve confinement by reducing turbulence.[3,4] Lower hybrid waves can be used for driving current to provide for plasma confinement,[5] which is particularly effective if the wave power can penetrate the plasma core. Early experiments utilizing externally launched microwave power in the lower hybrid frequency range were aimed at heating the plasma ions, and operated at relatively high plasma density (line-averaged density of about $1 \times 10^{20}\mathrm{m}^{-3}$).[6] In these experiments, the coupled radio-frequency (RF) power did not produce any effect in the plasma core, but remained deposited at the very edge.[7–10] More recently, a similar effect of lack of RF power penetration in the core was found in LHCD experiments approaching reactor graded conditions of high plasma density on FTU (Frascati Tokamak Upgrade)[11] and JET (Joint European Torus).[12] Consistently with FTU results, further LHCD experiments at high plasma density obtained effects of LH power deposition in the scrape-off layer, on Alcator C-Mod,[13] and decrease of the LHCD efficiency stronger than expected on Tore Supra.[14] By means of the interpretation of this phenomenon on the basis of parasitic absorption in the scrape-off layer produced by non-linear mechanism,[15] a new method for enabling the penetration of the coupled LH power in the core was assessed on FTU.[11] Recent studies have shown that the wave-particle interactions in the scrape-off layer diminish when the temperature of peripheral plasma electrons is high.[11,16] Therefore, externally launching radio frequency power coupled to lower hybrid waves is still a promising method of driving current and improving confinement for future tokamaks with high-density plasma, such as ITER.

In the experiments carried out in Alcator C-Mod, significant changes of toroidal rotation speed have been observed after the launch of lower hybrid waves for driving current. Counter-current toroidal rotation driven by lower hybrid waves was first reported by C-Mod team during lower hybrid current driving.[17,18] The total power coupled to lower hybrid waves was about 0.8 MW for Alcator C-Mod. The waves had been shown to induce a counter-current change in toroidal rotation of up to 60 km/s in the central region of the plasma ($r/a \lesssim 0.4$). Furthermore, the changes in the central rotation velocity were proven to be well correlated with changes in normalized internal inductance. This indicates current drive is responsible for the rotation profile modifications. In the follow-up studies,[19–21] lower hybrid waves were shown to be able to drive toroidal rotation in both counter-current and co-current direction. At a fixed density of $n_e \sim 0.66 \times 10^{20}\mathrm{m}^{-3}$, there existed a critical current, where the direction of toroidal rotation was reversed. During high current cases, e.g., 700 kA, the rotation drive was in the counter-current direction with a rotation change of $\sim -30\,\mathrm{km/s}$. At low current, e.g., 400 kA, the core rotation was driven in the co-current direction with $\Delta v \sim 30\,\mathrm{km/s}$.

Recently, different theoretical approaches have been adopted to explain plasma rotations with no external momentum input. A theory based on the turbulent momentum transport seems to be promising, in which it is believed that non-zero parallel Reynolds stress of turbulence is the force that drives toroidal flow.[22,23] Thermal-ion-loss at plasma edge is also suggested to be the reason of plasma intrinsic rotation.[24] In this theory, thermal ions moving in certain direction are easier to hit first wall than others, as a result extra momentum is left in plasma. There are a few theories exclusively for toroidal rotations observed during lower hybrid current driving (LHCD).[25,26] In these works, it is suggested that Ware pinch of trapped electrons induced by lower hybrid

waves is the major reason for the spin-up. However, there is no conclusive theoretical explanation of the toroidal rotations observed in Alcator C-Mod with LHCD, which is sensitive to the configuration of the lower hybrid waves and closely associated with wave-driven toroidal current. In this paper, we present a new theory to understand the rotations observed in Alcator C-Mod with LHCD. In our theory, the driving force of rotation is proportional to the magnitude of the wave-driven toroidal current and depends on the propagation of lower hybrid waves in plasma. In addition, this theory has the potential to be applied to toroidal rotations observed in other situations, e.g., plasmas with ICRF heating.[27,28]

The main idea of our theory is as follows. In the background magnetic field, lower hybrid waves push resonant electrons to drift across flux surfaces. This drift brings charge build-up in plasma and therefore formation of the radial electric field, which drives bulk electrons to flow across flux surfaces as a return current to counteract the charge accumulation. The Lorentz force on the return current of bulk electrons is the momentum source, which drives plasma to spin up. The momentum is transferred to ions by friction between bulk electrons and ions. The physics of driving return current across flux surfaces is a complicate issue itself. For certain cases, the return current can be carried by bulk ions and electrons together or even mainly ions. But the difference in the carriers of the return current does not change the magnitude and direction of the Lorentz force on the return current.

Two key points distinguish our theory from previous studies of plasma rotation. First, we believe that the Lorentz force brought by the bulk-electron flow across flux surfaces is the momentum source, which drives toroidal plasma rotation. In other theories, non-diffusive residual stress of momentum transport[22] or thermal-ion-orbit loss near edge[24] are the candidates to provide the momentum for toroidal plasma rotation. In addition, the bulk-electron flow is a response of the plasma to the resonant-electron flow across flux surfaces induced by lower hybrid waves. In previous theoretical studies,[29,30] effects of lower hybrid waves are considered solely to be driving current and heating.

Here, we briefly describe the physical picture of our theory. As explained above, the Lorentz force is the momentum source for toroidal plasma rotation in our model. If we use the two-fluid model to describe the plasma, the toroidal components of momentum equations are

$$n_e m_e \frac{\partial u_e^{\varphi}}{\partial t} + n_e m_e \mathbf{u_e} \cdot \frac{\partial u_e^{\varphi}}{\partial \mathbf{x}} = -(\nabla \cdot \Pi_e)^{\varphi} + n_e q_e (\mathbf{E}^{\varphi} + u_e^r \times \mathbf{B}^{\theta}) + \mathbf{f}_{ei}^{\varphi}, \quad (1)$$

$$n_i m_i \frac{\partial u_i^{\varphi}}{\partial t} + n_i m_i \mathbf{u_i} \cdot \frac{\partial u_i^{\varphi}}{\partial \mathbf{x}} = -(\nabla \cdot \Pi_i)^{\varphi} + n_i q_i (\mathbf{E}^{\varphi} + u_i^r \times \mathbf{B}^{\theta}) + \mathbf{f}_{ie}^{\varphi}, \quad (2)$$

where terms on the right-hand side of Eqs. (1) and (2) represent momentum transport, electric force, the Lorentz force, and friction, respectively. The driving force of rotation is one or multiple terms on the right-hand side of Eqs. (1) and (2). The Lorentz force in Eq. (1), $u_e^r \times \mathbf{B}^{\theta}$, can act on toroidal rotation of ions, u_i^{φ}, through friction. The bulk electron flow, u_e^r, is a response of the plasma to a resonant-electron flow across flux surfaces, which builds up charge hence the radial electric field. This resonant-electron flow is induced by the $\mathbf{E} \times \mathbf{B}$ drift due to the perpendicular electric field of the lower hybrid waves. It is well-known that the electric field of lower hybrid waves has parallel and perpendicular components, and the parallel electric field interacts with resonant electrons to drive current. However, the effects of the perpendicular electric field of the lower hybrid waves have been largely ignored so far.

In Sec. II, we will use kinetic equations to derive a set of fluid equations to describe the toroidal plasma rotation induced by lower hybrid waves. The resonant-electron flow across flux surfaces is an input parameter of the fluid equations that has to be calculated before we can solve the equations. In Sec. III, we will use an improved quasilinear theory to study the distribution function of resonant electrons during LHCD and to calculate magnitude and direction of the resonant-electron flow across flux surfaces. By substituting the results of Sec. III into the fluid equations in Sec. II, the set of fluid equations is completed. Using the completed fluid equations, we will study toroidal plasma rotation induced by lower hybrid waves in Sec. IV. Discussions are given in Sec. V.

II. FLUID EQUATIONS FOR LHCD INDUCED PLASMA ROTATION

In this section, we start from kinetic equations of ions and electrons to derive a set of fluid equations to study the rotation of a two-component plasma during the launch of lower hybrid waves. As discussed in the end of Sec. I, the resonant-electron flow across flux surfaces is an input parameter of the fluid equations, which has to be calculated before we can solve the fluid equations. Therefore, we divide the distribution function of electrons into that of resonant electrons and bulk electrons. We will use the distribution functions of bulk electrons and ions to derive the fluid equations and use the distribution function of resonant electrons to calculate resonant-electron flow across flux surfaces. This approximation has been adopted in previous study for RF current-drive theory.[30,31] Bulk electrons, i.e., those with speed $v \lesssim v_{et}$, all experience about the same collisionality with collision rate proportional to v_{et}^{-3}. Here v_{et} is thermal electron speed. Resonant electrons are those with speed $v \sim v_{LH} \gg v_{et}$, where v_{LH} is parallel phase velocity of the lower hybrid wave. Collision frequency of these electrons will be $(v_{et}/v_{LH})^3$ smaller than that for bulk electrons. In practise, even a resonant electron with $v_{et}/v \sim v_{et}/v_{LH} \simeq 1/3$ may be considered fast, hence relatively collisionless. Therefore, it is reasonable to separate resonant electrons from bulk electrons. By taking this approximation, we can take moments of the kinetic equations of bulk electrons and ions to derive the set of two-fluid equations.

Kinetic equations for ions and electrons are

$$\frac{\partial f_e}{\partial t} + \mathbf{v} \cdot \frac{\partial f_e}{\partial \mathbf{x}} + \frac{q_e}{m_e} (\mathbf{E} + \mathbf{v} \times \mathbf{B}) \cdot \frac{\partial f_e}{\partial \mathbf{v}} = C(f_e, f_e) + C(f_e, f_i), \quad (3)$$

$$\frac{\partial f_i}{\partial t}+\mathbf{v}\cdot\frac{\partial f_i}{\partial \mathbf{x}}+\frac{q_i}{m_i}(\mathbf{E}+\mathbf{v}\times\mathbf{B})\cdot\frac{\partial f_i}{\partial \mathbf{v}}=C(f_i,f_i)+C(f_i,f_e), \tag{4}$$

where C is collision operator. As discussed above, we divide f_e into $f_e=f_{enr}+f_{er}$ with the assumption that $f_{enr}\gg f_{er}$. Here, f_{enr} and f_{er} are distribution function of bulk (non-resonant) electrons and resonant electrons. Substituting $f_e=f_{enr}+f_{er}$ into Eqs. (3) and (4) and only keep dominant terms, we have kinetic equations for resonant electrons, bulk electrons and ions

$$\frac{\partial f_{er}}{\partial t}+\mathbf{v}\cdot\frac{\partial f_{er}}{\partial \mathbf{x}}+\frac{q_e}{m_e}(\mathbf{E}+\mathbf{v}\times\mathbf{B})\cdot\frac{\partial f_{er}}{\partial \mathbf{v}}=C(f_{er},f_{enr})+C(f_{enr},f_{er})+C(f_{er},f_i), \tag{5}$$

$$\frac{\partial f_{enr}}{\partial t}+\mathbf{v}\cdot\frac{\partial f_{enr}}{\partial \mathbf{x}}+\frac{q_e}{m_e}(\mathbf{E}+\mathbf{v}\times\mathbf{B})\cdot\frac{\partial f_{enr}}{\partial \mathbf{v}}=C(f_{enr},f_{enr})+C(f_{enr},f_i), \tag{6}$$

$$\frac{\partial f_i}{\partial t}+\mathbf{v}\cdot\frac{\partial f_i}{\partial \mathbf{x}}+\frac{q_i}{m_i}(\mathbf{E}+\mathbf{v}\times\mathbf{B})\cdot\frac{\partial f_i}{\partial \mathbf{v}}=C(f_i,f_i)+C(f_i,f_{enr}). \tag{7}$$

One can notice that the equations of bulk electrons and ions, Eqs. (6) and (7), seem to be decoupled from the equation of resonant electrons, Eq. (5). We will see later that the physics of resonant electrons and bulk electrons will be coupled by electromagnetic field. We will use Eq. (5) to calculate the resonant-electron flow across flux surfaces later in Sec. III. Now we take moments of Eqs. (6) and (7) to derive the two-fluid equations for bulk electrons and ions

$$\frac{\partial n_{enr}}{\partial t}+\frac{\partial}{\partial \mathbf{x}}\cdot(n_{enr}\mathbf{u_{enr}})=0, \tag{8}$$

$$\frac{\partial n_i}{\partial t}+\frac{\partial}{\partial \mathbf{x}}\cdot(n_i\mathbf{u_i})=0, \tag{9}$$

$$n_{enr}m_e\frac{\partial \mathbf{u_{enr}}}{\partial t}+n_{enr}m_e\mathbf{u_{enr}}\cdot\frac{\partial \mathbf{u_{enr}}}{\partial \mathbf{x}}=-\nabla\cdot\Pi_{\mathbf{enr}}-\nabla p_{enr}+q_e(\mathbf{E}_0+\mathbf{u_{enr}}\times\mathbf{B}_0)+\mathbf{f}_{enr,i}, \tag{10}$$

$$n_im_i\frac{\partial \mathbf{u_i}}{\partial t}+n_im_i\mathbf{u_i}\cdot\frac{\partial \mathbf{u_i}}{\partial \mathbf{x}}=-\nabla\cdot\Pi_{\mathbf{i}}-\nabla p_i+q_i(\mathbf{E}_0+\mathbf{u_i}\times\mathbf{B}_0)+\mathbf{f}_{i,enr}, \tag{11}$$

$$\frac{\partial \mathbf{p_{enr}}}{\partial t}+\mathbf{u_{enr}}\cdot\frac{\partial p_{enr}}{\partial \mathbf{x}}=-\gamma p_{enr}\nabla\cdot\mathbf{u_{enr}}, \tag{12}$$

$$\frac{\partial \mathbf{p_i}}{\partial t}+\mathbf{u_i}\cdot\frac{\partial p_i}{\partial \mathbf{x}}=-\gamma p_i\nabla\cdot\mathbf{u_i}. \tag{13}$$

Here $n_{enr}, n_i, \mathbf{u_{enr}}, \mathbf{u_i}, \Pi_{\mathbf{enr}}, \Pi_{\mathbf{i}}, p_{enr}$, and p_i are density, fluid velocity, viscosity, and pressure of bulk electrons and ions, respectively.

It is important to notice that the two-fluid equations are for bulk electrons and ions. Fast oscillating field of lower hybrid waves have no direct effects on bulk electrons and ions. Therefore, we have ignored the wave field and used the slow-changing background field $\mathbf{E}_0$ and $\mathbf{B}_0$ instead of the total field $\mathbf{E}$ and $\mathbf{B}$ in the equations. In addition, Eqs. (8)–(13) do not include resonant electrons directly. Resonant electrons act on bulk electrons and ions through electric field $\mathbf{E}_0$ and magnetic field $\mathbf{B}_0$. The current carried by resonant electrons changes $\mathbf{B}_0$ and the charge built up by the resonant-electron flow across flux surfaces generates radial component of $\mathbf{E}_0$. For this reason, we use Maxwell's equations of the background fields $\mathbf{E}_0$ and $\mathbf{B}_0$ to couple the physics of fields and particles

$$\nabla\cdot\mathbf{E_0}=\frac{q_en_{er}+q_en_{enr}+q_in_i}{\epsilon_0}, \tag{14}$$

$$\nabla\times\mathbf{E_0}=-\frac{\partial \mathbf{B_0}}{\partial t}, \tag{15}$$

$$\nabla\times\mathbf{B_0}-\mu_0\epsilon_0\frac{\partial \mathbf{E_0}}{\partial t}=\mu_0(q_en_{er}\mathbf{u_{er}}+q_en_{enr}\mathbf{u_{enr}}+q_in_i\mathbf{u_i}). \tag{16}$$

Here, n_{er} and $n_{er}\mathbf{u_{er}}$ denote resonant-electron density and flow. We can simplify the problem by assuming that background magnetic field is constant in the fluid equations. Thus, we can use Poisson's equation alone instead of the complete set of Maxwell's equations. The simplification can be justified by the following arguments. In experiments with LHCD, toroidal current is usually controlled by feedback system to be constant before and after the launch of lower hybrid waves. As a result, magnetic field is relatively constant except that the radial profile of poloidal magnetic field changes. Therefore, taking the background magnetic field as constant is a good approximation.

After assuming constant magnetic field, the set of fluid equations includes Eqs. (8)–(13) and (14), and they can be further simplified. Since toroidal rotation is our goal, we will start from the toroidal component of momentum equations

$$n_{enr}m_e\frac{\partial u^{\varphi}_{enr}}{\partial t}+n_{enr}m_e\mathbf{u_{enr}}\cdot\frac{\partial u^{\varphi}_{enr}}{\partial \mathbf{x}}=-(\nabla\cdot\Pi_{\mathbf{enr}})_{\varphi}+q_e(E^{\varphi}_0+u^r_{enr}B^{\theta}_0)+f^{\phi}_{enr,i}, \tag{17}$$

$$n_im_i\frac{\partial u^{\varphi}_i}{\partial t}+n_im_i\mathbf{u_i}\cdot\frac{\partial u^{\varphi}_i}{\partial \mathbf{x}}=-(\nabla\cdot\Pi_{\mathbf{i}})_{\varphi}+q_i(E^{\varphi}_0+u^r_iB^{\theta}_0)+f^{\phi}_{i,enr}. \tag{18}$$

We have neglected $(\nabla p_{enr})^{\varphi}$ and $(\nabla p_i)^{\varphi}$ in Eqs. (17) and (18) because of the toroidal symmetry of tokamak. Convective terms, which are second terms on the left-hand side of Eqs. (17) and (18), are typically small and can be ignored.[32,33] Toroidal electric field on the right-hand side of Eqs. (17) and (18) is close to zero during LHCD according to experimental observations.[34] We can also safely neglect u^r_i because ions response much more slowly to the radial electric field than electrons do. Viscosities of bulk electrons and ions, which are the first terms on the right-hand side of Eqs. (17) and (18), can be written as[35,36]

$$-(\nabla\cdot\Pi_{\mathbf{enr}})^{\varphi}=n_{enr}m_e\left(\chi_{enr}\frac{\partial^2u^{\varphi}_{enr}}{\partial r^2}+v_{enr}\frac{\partial u^{\varphi}_{enr}}{\partial r}\right), \tag{19}$$

$$-(\nabla\cdot\Pi_{\mathbf{i}})^{\varphi}=n_i m_i\left(\chi_i\frac{\partial^2 u_i^{\varphi}}{\partial r^2}+v_i\frac{\partial u_i^{\varphi}}{\partial r}\right), \tag{20}$$

where χ_{enr}, v_{enr}, χ_i, and v_i are momentum diffusivities and momentum-pinch velocities of bulk electrons and ions. Friction between bulk electrons and ions, $f^{\phi}_{enr,i}$ and $f^{\phi}_{i,enr}$, are defined as

$$f^{\phi}_{enr,i}=-f^{\phi}_{i,enr}=n_{enr}m_e\nu_{enr,i}(u^{\varphi}_{enr}-u^{\varphi}_i). \tag{21}$$

Here $\nu_{enr,i}$ is collision rate of bulk electrons on ions. If we assume that the time scale for the charge build-up to reach steady state is much faster than that for plasma rotation, the following equation holds while u_i^{φ} evolves:

$$\frac{\partial(q_e n_{er}+q_e n_{enr}+q_i n_i)}{\partial t}=-\nabla\cdot(q_e n_{er}\mathbf{u_{er}}+q_e n_{enr}\mathbf{u_{enr}}+q_i n_i\mathbf{u_i})=0. \tag{22}$$

Since it is the flow across flux surfaces that causes charge build-up, we can re-write Eq. (22) as

$$\frac{\partial(q_e n_{er}+q_e n_{enr})}{\partial t}=-\frac{1}{r}\frac{\partial}{\partial r}r(q_e n_{er}u^r_{er}+q_e n_{enr}u^r_{enr})=0. \tag{23}$$

Again, u_i^r in Eq. (23) has been neglected. With the boundary condition $u^r_{er}(r=a)=u^r_{enr}(r=a)=0$, where a is minor radius, Eq. (23) gives

$$n_{enr}u^r_{enr}=-n_{er}u^r_{er}. \tag{24}$$

Combining all the simplifications and definitions above, we have the toroidal momentum equations for bulk electrons and ions

$$n_{enr}m_e\frac{\partial u^{\varphi}_{enr}}{\partial t}=n_{enr}m_e\left(\chi_{enr}\frac{\partial^2 u^{\varphi}_{enr}}{\partial r^2}+v_{enr}\frac{\partial u^{\varphi}_{enr}}{\partial r}\right)-q_e n_{er}u^r_{er}B^{\theta}_0-n_{enr}m_e\nu_{enr,i}(u^{\varphi}_{enr}-u^{\varphi}_i), \tag{25}$$

$$n_i m_i\frac{\partial u^{\varphi}_i}{\partial t}=n_i m_i\left(\chi_i\frac{\partial^2 u^{\varphi}_i}{\partial r^2}+v_i\frac{\partial u^{\varphi}_i}{\partial r}\right)-n_{enr}m_e\nu_{enr,i}(u^{\varphi}_i-u^{\varphi}_{enr}). \tag{26}$$

If we take densities n_{enr} and n_i, momentum diffusivities χ_{enr} and χ_i, momentum-pinch velocities v_{enr} and v_i, resonant-electron flow across flux surfaces $n_{er}u^r_{er}$, and collision frequency $\nu_{enr,i}$ to be known quantities, we only have two unknown variables left, u^{φ}_{enr} and u^{φ}_i for two equations, Eqs. (25) and (26). Therefore, Eqs. (25) and (26) are complete and can be used to study toroidal rotation. This method has been adopted previously to study toroidal rotations.[33] The differences here are that we use toroidal momentum equations of both bulk electrons and ions instead of just one for ions, and there is a driving force $q_e n_{er}u^r_{er}B^{\theta}_0$ in the equation of bulk electrons. The magnitude and direction of $n_{er}u^r_{er}$ will be calculated in the next section. Another important feature of Eqs. (25) and (26) is the symmetry with respect to the signs of u^{φ}_{enr}, u^{φ}_i, and u^r_{er}. If $(u^{\varphi}_{enr},u^{\varphi}_i)$ is a solution of Eqs. (25) and (26) for a given resonant-electron flow across flux surfaces $n_{er}u^r_{er}$, it is not difficult to prove that $(-u^{\varphi}_{enr},-u^{\varphi}_i)$ is also a solution of the system if we change the sign of $n_{er}u^r_{er}$. Therefore, our approach theoretically allows the existence of opposite toroidal rotations.

III. LOWER HYBRID WAVES INDUCED RESONANT-ELECTRON FLOW ACROSS FLUX SURFACES

In this section, we calculate the resonant-electron flow across flux surfaces $n_{er}u^r_{er}$. Lower hybrid waves used in LHCD can not only drive toroidal current but also push resonant electrons to form a flow across flux surfaces. However, we cannot obtain this flow by following the standard quasilinear analysis for velocity-space diffusion caused by lower hybrid waves. Here we discuss the reason using the calculations in Refs. 29 and 37 as examples. Following these standard analysis, we calculate the velocity-space diffusion of resonant-electron distribution function in cylindrical coordinates for velocity and wave-vector

$$\begin{aligned}v_x&=v_\perp\cos\phi\quad v_y=v_\perp\sin\phi,\\ k_x&=k_\perp\cos\psi\quad k_y=k_\perp\sin\psi,\end{aligned} \tag{27}$$

where ϕ is the angle between x axis and perpendicular velocity, and ψ is the angle between x axis and perpendicular wave-vector. The background magnetic field $\mathbf{B}_0$ is chosen to be in the z-direction. Flow across flux surfaces is the first moment of the ϕ-dependent part of the distribution function as shown later in Eq.(58). But in Refs. 29 and 37, the distribution function is averaged over the period $[0,2\pi]$ in ϕ. The averaged distribution function only depends on parallel velocity v_z and perpendicular velocities $v_\perp$. By taking the first moment of the averaged distribution function, no flow across flux surfaces can be derived.

In order to correctly calculate the resonant-electron flow across flux surfaces, we do not average resonant-electron distribution function over ϕ. The distribution function of resonant electrons is expanded into Fourier components of ϕ

$$f=\sum_{n=-\infty}^{+\infty}f^n e^{in\phi}. \tag{28}$$

The first moment of the first harmonics $f^{\pm1}e^{\pm i\phi}$ gives the resonant-electron flow across flux surfaces $n_{er}u^r_{er}$. We will first carry out the calculation for general electromagnetic waves, and then the result is restricted to lower hybrid waves. Following quasilinear theory,[29,37] we split the distribution function of resonant electrons f_{er} into fluctuation and non-fluctuation parts denoted by $\tilde{f}_{er}$ and $f_{er,0}$, then substitute them into Eq. (5). The corresponding equations of $\tilde{f}_{er}$ and $f_{er,0}$ are

$$\frac{\partial\tilde{f}_{er}}{\partial t}+\mathbf{v}\cdot\frac{\partial\tilde{f}_{er}}{\partial\mathbf{x}}+\frac{q_e}{m_e}(\mathbf{v}\times\mathbf{B_0})\cdot\frac{\partial\tilde{f}_{er}}{\partial\mathbf{v}}=-\frac{q_e}{m_e}(\tilde{\mathbf{E}}+\mathbf{v}\times\tilde{\mathbf{B}})\cdot\frac{\partial f_{er,0}}{\partial\mathbf{v}}, \tag{29}$$

$$\frac{\partial f_{er,0}}{\partial t}+\frac{q_e}{m_e}(\mathbf{v}\times\mathbf{B_0})\cdot\frac{\partial f_{er,0}}{\partial \mathbf{v}}=C(f_{er,0},f_{enr})+C(f_{enr},f_{er,0})+C(f_{er,0},f_i)+\frac{\partial}{\partial \mathbf{v}}\cdot\left[-\frac{q_e}{m_e}(\tilde{\mathbf{E}}+\mathbf{v}\times\tilde{\mathbf{B}})\tilde{f}_{er}\right], \tag{30}$$

where $\mathbf{B_0}, \tilde{E}$, and $\tilde{B}$ are static magnetic field, electric field, and magnetic field of the electromagnetic waves. We have neglected static electric field in Eqs. (29) and (30) because contributions of static magnetic field and waves are dominant. Collision terms in Eq. (29) are dropped since the fluctuation part is mainly determined by waves and static magnetic field. For simplicity, we have ignored the spatial gradient of $f_{er,0}$ in Eq. (30) as well.

The last term on right-hand side of Eq. (30) is the velocity-space diffusion, which represents the effect of waves on electrons. We will solve Eq. (29) for $\tilde{f}_{er}$ through Fourier transform, then substitute it into the term of velocity-space diffusion to solve Eq. (30) for $f_{er,0}$. Fourier transforms of $\tilde{f}_{er}, \tilde{E}$, and $\tilde{B}$ are

$$\tilde{f}_{er}=\int_{\infty}^{\infty}\frac{d^3k}{(2\pi)^3}\tilde{f}_{er\mathbf{k}}e^{i(\mathbf{k}\cdot\mathbf{r}-\omega_{\mathbf{k}}t)}, \tag{31}$$

$$\tilde{\mathbf{E}}=\int_{\infty}^{\infty}\frac{d^3q}{(2\pi)^3}\tilde{\mathbf{E}}_{\mathbf{q}}e^{i(\mathbf{q}\cdot\mathbf{r}-\omega_{\mathbf{q}}t)}, \tag{32}$$

$$\tilde{\mathbf{B}}=\int_{\infty}^{\infty}\frac{d^3q}{(2\pi)^3}\tilde{\mathbf{B}}_{\mathbf{q}}e^{i(\mathbf{q}\cdot\mathbf{r}-\omega_{\mathbf{q}}t)}. \tag{33}$$

It is convenient to use rotating coordinates for the wave field components in the form

$$\begin{aligned}\tilde{E}^{\pm}&=\tilde{E}_x\pm i\tilde{E}_y,\\ \tilde{B}^{\pm}&=\tilde{B}_x\pm i\tilde{B}_y.\end{aligned} \tag{34}$$

Using these expressions, we can write the Fourier-transformed Eq. (29) and (30) as

$$-i\omega_{\mathbf{k}}\tilde{f}_{er,\mathbf{k}}+i[k_zv_z+k_\perp v_\perp\cos(\phi-\psi)]\tilde{f}_{er,\mathbf{k}}-\omega_{ce}\frac{\partial\tilde{f}_{er,\mathbf{k}}}{\partial\phi}=-\frac{q_e}{m_e}(\tilde{\mathbf{E}}_{\mathbf{k}}+\mathbf{v}\times\tilde{\mathbf{B}}_{\mathbf{k}})\cdot\frac{\partial f_{er,0}}{\partial\mathbf{v}}, \tag{35}$$

$$\frac{\partial f_{er,0}}{\partial t}+\frac{q_e}{m_e}(\mathbf{v}\times\mathbf{B_0})\cdot\frac{\partial f_{er,0}}{\partial\mathbf{v}}=C(f_{er,0},f_{enr})+C(f_{enr},f_{er,0})+C(f_{er,0},f_i)+\frac{\partial}{\partial\mathbf{v}}\cdot\int_{\mathbf{k}}\frac{d^3k}{(2\pi)^3}\times\left[-\frac{q_e}{m_e}(\tilde{\mathbf{E}}_{-\mathbf{k}}+\mathbf{v}\times\tilde{\mathbf{B}}_{-\mathbf{k}})\tilde{f}_{er,\mathbf{k}}\right]. \tag{36}$$

Equation (35) is a first-order differential equation in φ, the solution of which is

$$\begin{aligned}\tilde{f}_{er,\mathbf{k}}=\sum_{m,n=-\infty}^{+\infty}&J_m\left(\frac{k_\perp v_\perp}{\omega_{\mathbf{k}}}\right)J_n\left(\frac{k_\perp v_\perp}{\omega_{\mathbf{k}}}\right)\exp[i(n-m)\psi]\left(-\frac{q_s}{m_s}\right)\left[\frac{i}{\omega_{\mathbf{k}}-(n-1)\omega_{ce}-k_zv_z}\frac{\exp[i(m-n+1)\varphi]}{2}\right.\\&\times\left(E^-_{\mathbf{k}}\hat{\mathbf{G}}^+_{\mathbf{k}}+\frac{k_\perp E^z_{\mathbf{k}}}{\omega_{\mathbf{k}}}e^{-i\psi}\hat{\mathbf{H}}^+\right)\frac{i}{\omega_{\mathbf{k}}-(n+1)\omega_{ce}-k_zv_z}\frac{\exp[i(m-n-1)\varphi]}{2}\\&\times\left(E^+_{\mathbf{k}}\hat{\mathbf{G}}^-_{\mathbf{k}}+\frac{k_\perp E^z_{\mathbf{k}}}{\omega_{\mathbf{k}}}e^{+i\psi}\hat{\mathbf{H}}^-\right)\frac{ik_\perp}{2\omega_{\mathbf{k}}}(E^+_{\mathbf{k}}e^{-i\psi}-E^-_{\mathbf{k}}e^{+i\psi})v_\perp\hat{\mathbf{e}}_\phi\\&\left.+\frac{i}{\omega_{\mathbf{k}}-n\omega_{ce}-k_zv_z}\exp[i(m-n)\varphi]E^z_{\mathbf{k}}\hat{\mathbf{e}}_{v_z}\right]\cdot\frac{\partial f_{er,0}}{\partial\mathbf{v}},\end{aligned} \tag{37}$$

where J_n denotes nth order Bessel function of the first kind and

$$\begin{aligned}\hat{\mathbf{G}}^{\pm}_{\mathbf{k}}&\equiv\hat{\mathbf{e}}_{v_\perp}\pm i\hat{\mathbf{e}}_\phi-\frac{k_z}{\omega_{\mathbf{k}}}\hat{\mathbf{H}}^{\pm},\\ \hat{\mathbf{H}}^{\pm}&\equiv v_z\hat{\mathbf{e}}_{v_\perp}-v_\perp\hat{\mathbf{e}}_{v_z}\pm iv_z\hat{\mathbf{e}}_\phi.\end{aligned} \tag{38}$$

Following our procedure discussed above, we will substitute the solution $\tilde{f}_{er,\mathbf{k}}$ into the term of velocity-space diffusion in Eq. (36) to solve for $f_{er,0}$. As mentioned after Eq. (28), we only need the first harmonics of the Fourier-transformed $f_{er,0}$ to calculate the resonant-electron flow across flux surfaces. Hence, we keep equations for the zeroth and the first harmonics, $f^0_{er,0}$ and $f^{\pm1}_{er,0}$

$$\frac{\partial f^0_{er,0}}{\partial t}=C(f^0_{er,0})+\frac{\partial}{\partial\mathbf{v}}\cdot\mathbf{D}^{0\phi}\cdot\frac{\partial f^0_{er0}}{\partial\mathbf{v}}, \tag{39}$$

$$\frac{\partial f^1_{er,0}e^{i\phi}}{\partial t}-\omega_{ce}\frac{\partial f^1_{er,0}e^{i\phi}}{\partial\phi}=\frac{\partial}{\partial\mathbf{v}}\cdot\mathbf{D}^{i\phi}\cdot\frac{\partial f^0_{er0}}{\partial\mathbf{v}}, \tag{40}$$

$$\frac{\partial f^{-1}_{er0}e^{-i\phi}}{\partial t}-\omega_{ce}\frac{\partial f^{-1}_{er0}e^{-i\phi}}{\partial\phi}=\frac{\partial}{\partial\mathbf{v}}\cdot\mathbf{D}^{-i\phi}\cdot\frac{\partial f^0_{er0}}{\partial\mathbf{v}}, \tag{41}$$

where $C(f^0_{er,0})\equiv C(f^0_{er,0},f_{enr})+C(f_{enr},f^0_{er,0})+C(f^0_{er,0},f_i)$ and the velocity-space diffusion tensors $\mathbf{D}^{0\phi}, \mathbf{D}^{i\phi}$, and $\mathbf{D}^{-i\phi}$ are

$$\mathbf{D}^{0\phi} = \frac{q_e^2}{m_e^2}\sum_{n=-\infty}^{+\infty}\frac{1}{V}\int\frac{d^3k}{(2\pi)^3}\frac{i}{\omega_{\mathbf{k}} - n\omega_{ce} - k_z v_z}\mathbf{a}_{nk}^*\mathbf{a}_{nk}, \quad (42)$$

$$\mathbf{D}^{i\phi} = \frac{q_e^2}{m_e^2}\sum_{n=-\infty}^{+\infty}\frac{1}{V}\int\frac{d^3k}{(2\pi)^3}\frac{ie^{i\phi}}{\omega_{\mathbf{k}} - n\omega_{ce} - k_z v_z}\mathbf{b}_{1nk}^*\mathbf{c}_{1nk}, \quad (43)$$

$$\mathbf{D}^{-i\phi} = \frac{q_e^2}{m_e^2}\sum_{n=-\infty}^{+\infty}\frac{1}{V}\int\frac{d^3k}{(2\pi)^3}\frac{ie^{-i\phi}}{\omega_{\mathbf{k}} - n\omega_{ce} - k_z v_z}\mathbf{b}_{-1nk}^*\mathbf{c}_{-1nk}, \quad (44)$$

with

$$\begin{aligned}\mathbf{a}_{nk} = {}& \frac{1}{2}\left(E_{\mathbf{k}}^+\mathbf{g}_{\mathbf{k}} + \frac{k_\perp E_{\mathbf{k}}^z}{\omega_{\mathbf{k}}}e^{i\psi}\mathbf{h}\right)e^{-i\psi}J_{n-1}\left(\frac{k_\perp v_\perp}{\omega_c}\right)\\ &+\frac{1}{2}\left(E_{\mathbf{k}}^-\mathbf{g}_{\mathbf{k}} + \frac{k_\perp E_{\mathbf{k}}^z}{\omega_{\mathbf{k}}}e^{-i\psi}\mathbf{h}\right)e^{i\psi}J_{n+1}\left(\frac{k_\perp v_\perp}{\omega_c}\right)\\ &+E_k^z\hat{\mathbf{e}}_{vz}J_n\left(\frac{k_\perp v_\perp}{\omega_c}\right), \end{aligned} \quad (45)$$

$$\begin{aligned}\mathbf{b}_{1nk} = {}& \frac{1}{2}\left(E_{\mathbf{k}}^+\mathbf{G}_{\mathbf{k}}^- + \frac{k_\perp E_{\mathbf{k}}^z}{\omega_{\mathbf{k}}}e^{i\psi}\mathbf{H}^-\right)J_n\left(\frac{k_\perp v_\perp}{\omega_c}\right)\\ &+\frac{1}{2}\left(E_{\mathbf{k}}^-\mathbf{G}_{\mathbf{k}}^+ + \frac{k_\perp E_{\mathbf{k}}^z}{\omega_{\mathbf{k}}}e^{-i\psi}\mathbf{H}^+\right)e^{i2\psi}J_{n+2}\left(\frac{k_\perp v_\perp}{\omega_c}\right)\\ &+\left(\frac{ik_\perp v_\perp}{2\omega_{\mathbf{k}}}\left(E_{\mathbf{k}}^+e^{-i\psi} - E_{\mathbf{k}}^-e^{i\psi}\right)\hat{\mathbf{e}}_\phi + E_k^z\hat{\mathbf{e}}_{vz}\right)\\ &\times e^{i\psi}J_{n+1}\left(\frac{k_\perp v_\perp}{\omega_c}\right), \end{aligned} \quad (46)$$

$$\begin{aligned}\mathbf{b}_{-1nk} = {}& \frac{1}{2}\left(E_{\mathbf{k}}^+\mathbf{G}_{\mathbf{k}}^- + \frac{k_\perp E_{\mathbf{k}}^z}{\omega_{\mathbf{k}}}e^{i\psi}\mathbf{H}^-\right)e^{-2i\psi}J_{n-2}\left(\frac{k_\perp v_\perp}{\omega_c}\right)\\ &+\frac{1}{2}\left(E_{\mathbf{k}}^-\mathbf{G}_{\mathbf{k}}^+ + \frac{k_\perp E_{\mathbf{k}}^z}{\omega_{\mathbf{k}}}e^{-i\psi}\mathbf{H}^+\right)J_n\left(\frac{k_\perp v_\perp}{\omega_c}\right)\\ &+\left(\frac{ik_\perp v_\perp}{2\omega_{\mathbf{k}}}\left(E_{\mathbf{k}}^+e^{-i\psi} - E_{\mathbf{k}}^-e^{i\psi}\right)\hat{\mathbf{e}}_\phi + E_k^z\hat{\mathbf{e}}_{vz}\right)\\ &\times e^{-i\psi}J_{n-1}\left(\frac{k_\perp v_\perp}{\omega_c}\right), \end{aligned} \quad (47)$$

$$\begin{aligned}\mathbf{c}_{1nk} = \mathbf{c}_{-1nk} = {}& \frac{1}{2}\left(E_{\mathbf{k}}^+\mathbf{G}_{\mathbf{k}}^- + \frac{k_\perp E_{\mathbf{k}}^z}{\omega_{\mathbf{k}}}e^{i\psi}\mathbf{H}^-\right)e^{-i\psi}J_{n-1}\left(\frac{k_\perp v_\perp}{\omega_c}\right)\\ &+\frac{1}{2}\left(E_{\mathbf{k}}^-\mathbf{G}_{\mathbf{k}}^+ + \frac{k_\perp E_{\mathbf{k}}^z}{\omega_{\mathbf{k}}}e^{-i\psi}\mathbf{H}^+\right)e^{i\psi}J_{n+1}\left(\frac{k_\perp v_\perp}{\omega_c}\right)\\ &+\left(\frac{ik_\perp v_\perp}{2\omega_{\mathbf{k}}}\left(E_{\mathbf{k}}^+e^{-i\psi} - E_{\mathbf{k}}^-e^{i\psi}\right)\hat{\mathbf{e}}_\phi + E_k^z\hat{\mathbf{e}}_{vz}\right)J_n\left(\frac{k_\perp v_\perp}{\omega_c}\right), \end{aligned} \quad (48)$$

$$\mathbf{g}_{\mathbf{k}} = \hat{\mathbf{e}}_{v_\perp} - \frac{k_z}{\omega_{\mathbf{k}}}(v_z\hat{\mathbf{e}}_{v_\perp} - v_\perp\hat{\mathbf{e}}_{vz}), \quad (49)$$

$$\mathbf{h} = v_z\hat{\mathbf{e}}_{v_\perp} - v_\perp\hat{\mathbf{e}}_{vz}. \quad (50)$$

We have dropped the collision terms in Eqs. (40) and (41) by assuming that $f_{er,0}^0 \gg f_{er,0}^{\pm1}$. The physics of the zeroth harmonic $f_{er,0}^0$ in Eq. (39) has been well studied,[29,37] but the physics of the first harmonic $f_{er,0}^{\pm1}$ in Eqs. (40) and (41) has not. Heating and current-driving effects of electromagnetic waves are reflected in the velocity-space diffusion tensor $\mathbf{D}^{0\phi}$ in Eq. (39) since the tensor only contains velocity-diffusion in the $\hat{\mathbf{e}}_{v_\perp}$ and $\hat{\mathbf{e}}_{v_z}$ directions. For example, if we take $\mathbf{E}_{\mathbf{k}} = i\mathbf{k}\Phi$ and $n=0$ for $\mathbf{D}^{0\phi}$, which is the case for lower hybrid waves in LHCD, the only component left in $\mathbf{D}^{0\phi}$ is $\hat{\mathbf{e}}_{v_z}\hat{\mathbf{e}}_{v_z}$. This is exactly the diffusion coefficient used in LHCD theory.[30,31]

Using the expressions for the velocity-space diffusion tensors in Eqs. (42)–(44), we can solve Eqs. (40) and (41) for the first harmonics of the resonant-electron distribution function $f_{er,0}^1e^{i\phi}$ and $f_{er,0}^{-1}e^{-i\phi}$. Multiplying Eqs. (40) and (41) by $e^{-i\phi}$ and $e^{i\phi}$, we have equations for $f_{er,0}^{\pm1}$

$$\frac{\partial f_{er,0}^1}{\partial t} - i\omega_{ce}f_{er,0}^1 = P^1, \quad (51)$$

$$\frac{\partial f_{er,0}^{-1}}{\partial t} + i\omega_{ce}f_{er,0}^{-1} = P^{-1}, \quad (52)$$

with

$$P^1 \equiv e^{-i\phi}\frac{\partial}{\partial\mathbf{v}}\cdot\mathbf{D}^{i\phi}\cdot\frac{\partial f_{er,0}^0}{\partial\mathbf{v}} \quad P^{-1} \equiv e^{i\phi}\frac{\partial}{\partial\mathbf{v}}\cdot\mathbf{D}^{-i\phi}\cdot\frac{\partial f_{er,0}^0}{\partial\mathbf{v}}. \quad (53)$$

The solutions of Eqs. (51) and (52) are

$$f_{er,0}^1 = e^{i\omega_{ce}t}\int_0^t dt'e^{-i\omega_{ce}t'}P^1, \quad (54)$$

$$f_{er,0}^{-1} = e^{-i\omega_{ce}t}\int_0^t dt'e^{i\omega_{ce}t'}P^{-1}, \quad (55)$$

with the initial condition that $f_{er,0}^{\pm1} = 0$ at $t=0$. We need time-averaged distribution functions to calculate the resonant-electron flow across flux surfaces. The averages of $f_{er,0}^1$ and $f_{er,0}^1$ in one gyro-period at moment t are

$$\begin{aligned}\overline{f_{er,0}^1} &= \frac{1}{T}\left(\int_0^{t+T}dt'f_{er,0}^1 - \int_0^t dt'f_{er,0}^1\right) = -\frac{P^1}{i\omega_{ce}} + \frac{1}{\omega_{ce}^2}\frac{dP^1}{dt}\\ &\approx -\frac{P^1}{i\omega_{ce}}, \end{aligned} \quad (56)$$

$$\begin{aligned}\overline{f_{er,0}^{-1}} &= \frac{1}{T}\left(\int_0^{t+T}dt'f_{er,0}^{-1} - \int_0^t dt'f_{er,0}^{-1}\right) = \frac{P^{-1}}{i\omega_{ce}} + \frac{1}{\omega_{ce}^2}\frac{dP^{-1}}{dt}\\ &\approx \frac{P^{-1}}{i\omega_{ce}}, \end{aligned} \quad (57)$$

where T is one gyro-period. We have dropped $1/\omega_{ce}^2(dP^{\pm1}/dt)$ in above solutions of $\overline{f_{er,0}^1}$ and $\overline{f_{er,0}^{-1}}$, because $(dP^{\pm1}/dt)/P^{\pm1} \ll \omega_{ce}$. The resonant-electron flow across flux surfaces can be calculated by taking the first moment of $\overline{f_{er,0}^1}e^{i\phi} + \overline{f_{er,0}^{-1}}e^{-i\phi}$,

$$\begin{aligned}n_{er}u_{er}^r &= \int d^3v v_r\left(\overline{f_{er,0}^1}e^{i\phi} + \overline{f_{er,0}^{-1}}e^{-i\phi}\right)\\ &= \int d^3v v_r\left(\frac{-P^1e^{i\phi} + P^{-1}e^{-i\phi}}{i\omega_{ce}}\right). \end{aligned} \quad (58)$$

Equation (58) is correct for general electromagnetic waves. Now we apply Eq. (58) to lower hybrid waves for LHCD to calculate the resonant-electron flow across flux surfaces induced by lower hybrid waves.

In order to avoid the mathematical complexity of tokamak geometry, we carry out the calculation in a slab geometry shown in Fig. 1.

In this geometry, plasma exists in the region of $0 < y < a$. A constant and uniform magnetic field $\mathbf{B}_0$ is in z direction, and lower hybrid waves propagate within the x–z plane. Here the $-y$ direction in slab geometry is the counterpart of the r direction in tokamak geometry. We first calculate $n_{er}u_{er}^{y}$ using the following equation:

$$n_{er}u_{er}^{y} = \int d^3v v_\perp \sin\phi \left(\frac{-P^1 e^{i\phi} + P^{-1}e^{-i\phi}}{i\omega_{ce}}\right), \tag{59}$$

then consider it approximately the same as $-n_{er}u_{er}^{r}$. In order to calculate $n_{er}u_{er}^{y}$, we need to know $P^{\pm 1}$. As shown in Eq. (53), $P^{\pm 1}$ are functions of the velocity-diffusion tensors $\mathbf{D}^{\pm i\phi}$ and the zeroth harmonic of the distribution function $f_{er,0}^{0}$. We have to derive the expressions for $\mathbf{D}^{\pm i\phi}$ and $f_{er,0}^{0}$ first. For lower hybrid waves in LHCD, we have $\mathbf{E}_\mathbf{k} = i\mathbf{k}\Phi$ and $n = 0$ in the expressions of velocity-space diffusion tensors $\mathbf{D}^{0\phi}$, $\mathbf{D}^{i\phi}$, and $\mathbf{D}^{-i\phi}$, which can be written as

$$\mathbf{D}^{0\phi} = \frac{q_e^2}{m_e^2}\frac{1}{V}\int \frac{d^3k}{(2\pi)^3}\frac{iJ_0J_0}{\omega_\mathbf{k} - k_z v_z} E_k^{z*} E_k^z \hat{\mathbf{e}}_{v_z}\hat{\mathbf{e}}_{v_z}, \tag{60}$$

$$\mathbf{D}^{i\phi} = \frac{q_e^2}{m_e^2}\frac{1}{V}\int \frac{d^3k}{(2\pi)^3}\frac{ie^{i\phi}J_0J_0}{\omega_\mathbf{k} - k_z v_z}\frac{1}{2}\left[E_\mathbf{k}^x \mathbf{G}_\mathbf{k}^- + \frac{k_\perp E_\mathbf{k}^z}{\omega_\mathbf{k}}\mathbf{H}^-\right]^* E_\mathbf{k}^z \hat{\mathbf{e}}_{v_z}, \tag{61}$$

$$\mathbf{D}^{-i\phi} = \frac{q_e^2}{m_e^2}\frac{1}{V}\int \frac{d^3k}{(2\pi)^3}\frac{ie^{-i\phi}J_0J_0}{\omega_\mathbf{k} - k_z v_z}\frac{1}{2}\left[E_\mathbf{k}^x \mathbf{G}_\mathbf{k}^+ + \frac{k_\perp E_\mathbf{k}^z}{\omega_\mathbf{k}}\mathbf{H}^+\right]^* E_\mathbf{k}^z \hat{\mathbf{e}}_{v_z}. \tag{62}$$

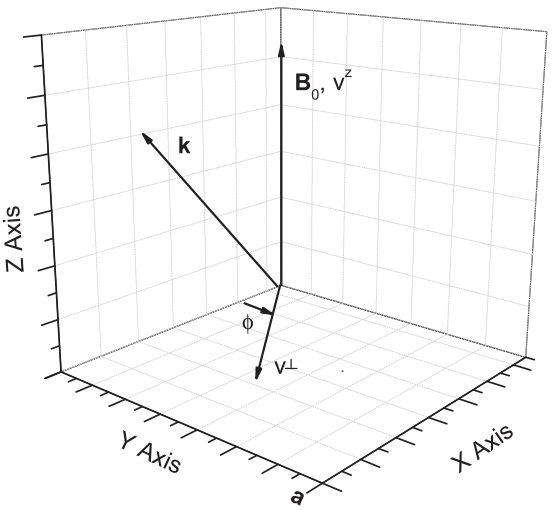

FIG. 1. Plasma exists in the region of $0 < y < a$. A constant and uniform magnetic field is in z direction, and lower hybrid waves propagate within the x–z plane.

Since the distribution function is approximately Maxwellian in the perpendicular direction, $k_\perp v_\perp/\omega_\mathbf{k} < 1$ holds for majority of the electrons. Therefore, all terms related to $J_{\pm 1,\pm 2}$ have been dropped in Eqs. (60)–(62), considering $J_{\pm 1,\pm 2}(k_\perp v_\perp/\omega_\mathbf{k}) \ll J_0(k_\perp v_\perp/\omega_\mathbf{k})$ when $k_\perp v_\perp/\omega_\mathbf{k} < 1$. Substituting $\mathbf{D}^{0\phi}$, $\mathbf{D}^{i\phi}$, and $\mathbf{D}^{-i\phi}$ into Eq. (53) for $P^{\pm 1}$, we have

$$P^1 = P^{-1} = \frac{q_e^2}{m_e^2}\frac{1}{V}\int \frac{d^3k}{(2\pi)^3}\left[\frac{1}{v_\perp}\frac{\partial}{\partial v_\perp}v_\perp - \frac{1}{v_\perp}\right] \times \frac{iJ_0J_0}{\omega_\mathbf{k} - k_z v_z}\frac{E_\mathbf{k}^{x*}E_\mathbf{k}^z}{2}\frac{\partial f_{er,0}^0}{\partial v_z}. \tag{63}$$

In Eq. (63), we have neglected terms proportional to $k_z v_z/\omega_\mathbf{k}$ and $k_z v_\perp/\omega_\mathbf{k}$ since the parallel phase velocity of lower hybrid waves is large compared to the electron thermal velocity. The last step before we can use $P^{\pm 1}$ to calculate the resonant-electron flow across flux surfaces is to determine $f_{er,0}^0$. In the LHCD theory,[30,31] an analytical solution of $f_{er,0}^0$ is obtained using a one-dimensional theory

$$f_{er,0}^0 = C\exp\left[-\frac{v_\perp^2}{v_{et}^2}\right] \times \exp\left[\frac{1}{v_{et}^2}\int_0^{v_z} -dv_z' v_z' \Big/ \left(1 + \frac{v_z'^3}{v_{et}^3}\frac{D^{0\phi}(v_z')}{(2+Z_{eff})v_{et}^2\nu_{enr,i}}\right)\right], \tag{64}$$

where v_{et} is the thermal velocity of bulk electrons, and C is an integration constant. The velocity-diffusion tensor $\mathbf{D}^{0\phi}$ in Eq. (64) is usually assumed to be[30,31]

$$\mathbf{D}^{0\phi} = D^{0\phi}(v_z)\hat{\mathbf{e}}_{v_z}\hat{\mathbf{e}}_{v_z}, \tag{65}$$

with

$$D^{0\phi}(v_z) = \begin{cases} D^{0\phi}, & V_{LH1} \le v_z \le V_{LH2}; \\ 0, & v_z < V_{LH1} \text{ or } V_{LH2} < v_z. \end{cases} \tag{66}$$

Here V_{LH2} and V_{LH1} are the upper and lower limit of the parallel phase velocity. Usually, $D^{0\phi}$ is considered to be constant and $V_{LH1} \approx V_{LH2} = V_{LH}$. Spread of the parallel phase velocity ΔV_{LH} is defined as $V_{LH2} - V_{LH1}$, which satisfies $\Delta V_{LH} \ll V_{LH}$. Parallel velocities of resonant electrons satisfy $V_{LH1} \le v_z \le V_{LH2}$. Substituting $f_{er,0}^0$ in Eq. (64) into $P^{\pm 1}$ in Eq. (63), we have

$$P^1 = P^{-1} = -C\nu_{enr,i}(2+Z_i)\frac{v_{et}^3}{v_z^2}\left[\frac{1}{v_\perp}\frac{\partial}{\partial v_\perp}v_\perp - \frac{1}{v_\perp}\right] \times \exp\left(-\frac{v_\perp^2}{v_{et}^2}\right)\frac{q_e^2}{m_e^2}\frac{1}{V}\int \frac{d^3k}{(2\pi)^3}\frac{iJ_0J_0}{\omega_\mathbf{k} - k_z v_z}\frac{E_\mathbf{k}^{x*}E_\mathbf{k}^z}{2} \Big/ D^{0\phi}. \tag{67}$$

We need to know the integral

$$\frac{q_e^2}{m_e^2}\frac{1}{V}\int \frac{d^3k}{(2\pi)^3}\frac{iJ_0J_0}{\omega_\mathbf{k} - k_z v_z}\frac{E_\mathbf{k}^{x*}E_\mathbf{k}^z}{2} \Big/ D^{0\phi}$$

in Eq. (67) before we can use the equation to calculate the resonant-electron flow across flux surfaces. Using the definition of $\mathbf{D}^{0\phi}$ in Eq. (60), we can write the above integral as

$$\frac{1}{2}\frac{q_e^2}{m_e^2}\frac{1}{V}\int\frac{d^3k}{(2\pi)^3}\frac{iJ_0J_0}{\omega_{\mathbf{k}}-k_zv_z}E_{\mathbf{k}}^{x*}E_{\mathbf{k}}^{z}\Big/\frac{q_e^2}{m_e^2}\frac{1}{V}\int\frac{d^3k}{(2\pi)^3}\frac{iJ_0J_0}{\omega_{\mathbf{k}}-k_zv_z}E_k^{z*}E_k^{z},$$

which can be estimated to be $E_{\mathbf{k}}^x/2E_{\mathbf{k}}^z = k_x/2k_z$. As a result, $P^{\pm1}$ can be written as

$$P^1 = P^{-1} = -C\frac{(2+Z_{eff})}{2}\nu_{enr,i}\frac{k_x}{k_z}\frac{v_{et}^3}{v_z^2}\left[\frac{1}{v_\perp}\frac{\partial}{\partial v_\perp}v_\perp - \frac{1}{v_\perp}\right]\times\exp\left(-\frac{v_\perp^2}{v_{et}^2}\right). \quad (68)$$

At last, we can use $P^{\pm1}$ to calculate the resonant-electron flow across flux surfaces. Substituting $P^{\pm1}$ into Eq. (59), we have

$$n_{er}u_{er}^y = -C\pi(2+Z_{eff})\frac{\nu_{enr,i}}{\omega_{ec}}\frac{k_x}{k_z}\frac{v_{et}^5\Delta V_{LH}}{V_{LH}^2}. \quad (69)$$

Since resonant electrons only exist in the resonant region of velocity space, which is $V_{LH1} \le v_z \le V_{LH2}$, the integration in Eq. (59) is only needed to be completed in this region. The integral constant C can be determined by the wave-driven current in z direction

$$J_z^{LH} = q_e\int d^3v f_{er,0}^0 v_z = q_eC\pi v_{et}^2V_{LH}\Delta V_{LH}. \quad (70)$$

Combining Eqs. (69) and (70), we have the resonant-electron flow across flux surfaces

$$q_en_{er}u_{er}^y = -\frac{k_x}{k_z}\frac{(2+Z_{eff})}{V_{LH}^3/v_{et}^3}\frac{\nu_{enr,i}}{\omega_{ec}}J_z^{LH}. \quad (71)$$

As discussed previously, we can write resonant-electron flow across flux surfaces in tokamak geometry approximately as

$$q_en_{er}u_{er}^r \approx -q_en_{er}u_{er}^y = \frac{k_\perp}{k_\parallel}\frac{(2+Z_{eff})}{V_{LH}^3/v_{et}^3}\frac{\nu_{enr,i}}{\omega_{ec}}J_\parallel^{LH}, \quad (72)$$

where $J_\parallel^{LH}$ is plasma current measurable in experiments. It is important to pay attention to the factor $k_\perp$ in Eq. (72). This factor shows that propagation of lower hybrid waves in plasma determines the direction of the resonant-electron flow across flux surfaces if other terms in Eq. (72) are fixed. With the symmetry of Eqs. (25) and (26) discussed in Sec. II, our theory predicts opposite toroidal rotations given opposite $k_\perp$. In studies of propagation of lower hybrid waves in tokamaks,[38,39] there is no restriction for the sign of $k_\perp$, which in experiments might depend on the configuration of the discharge. In the next section, we will substitute the result in Eq. (72) into Eqs. (25) and (26) to study the toroidal rotation induced by lower hybrid waves.

IV. LHCD INDUCED PLASMA ROTATION

In this section, we will numerically solve Eqs. (25) and (26) for the toroidal rotation of ions. As discussed in Sec. II, we take densities n_{enr} and n_i, momentum diffusivities χ_{enr} and χ_i, momentum-pinch velocities v_{enr} and v_i, resonant-electron flow across flux surfaces $q_en_{er}u_{er}^r$, poloidal magnetic field B_0^θ, and collision frequency $\nu_{enr,i}$ as known quantities. For simplicity, we assume flat radial profiles for these quantities except for B_0^θ, v_{enr}, v_i, and $q_en_{er}u_{er}^r$. The input parameters for calculation have to be consistent with experimental data. From the reports of Alcator C-Mod,[17,18] we know electron density and temperature at plasma core are about $10^{20}/\mathrm{m}^3$ and 2.5 keV. Therefore we choose $n_{enr} = n_i = 10^{20}/\mathrm{m}^3$ and estimate the collision frequency of thermal electrons as $\nu_{enr,i} = 10^5/\mathrm{s}$. To determine the radio profile of the poloidal magnetic field B_0^θ, we simply assume a geometry with circular flux surfaces and a large aspect ratio with $B_0^\theta = rB_0/qR_0$. The magnitudes of axial magnetic field, major radius, minor radius, and interior safety factor of Alcator C-Mod have been listed in Ref. 40. We use a set of typical values for the calculation, which are $B_0 = 5\,\mathrm{T}, R_0 = 0.67\,\mathrm{m}, a = 0.21\,\mathrm{m}$, and $q = 1.5$. The momentum transport coefficients of tokamak plasma are still an unsolved issue. The momentum diffusivity, χ, is generally found to be similar to the ion thermal conductivity,[33] which is in the range of $0.05 \sim 0.5\,\mathrm{m}^2/\mathrm{s}$.[33,40] Hence, we use a diffusivity somewhat in the middle of the range, $\chi_{enr} = \chi_i = 0.225\ \mathrm{m}^2/\mathrm{s}$. For momentum-pinch velocities, theoretical results of either turbulent equipartition pinch[35,36] or fluid treatment[41] do not agree with the experiment observations, which is in the range of $0 \sim 6\,\mathrm{m/s}$.[40] We select a pinch-velocity in the middle approximately and assume a radial profile, so that $v_i = v_{enr} = 4\exp[-(r/a-0.4)^2/20]\ \mathrm{m/s}$. The resonant-electron flow across flux surfaces $q_en_{er}u_{er}^r$ is calculated using Eq. (72). The parallel phase velocity is usually $3 \sim 5$ times of electron thermal velocity in order to have a high driving efficiency.[30] The current driven by lower hybrid waves can typically reach the level of $3\,\mathrm{MA/m}^2$.[40] As a result, it is reasonable to choose $J_\parallel^{LH}$ and V_{LH}/v_{te} to be $2\times10^6\,\mathrm{A/m}^2$ and 4. Effective ion charge is selected as $Z_{eff} = 2.0$. We estimate ω_{ec} to be $8.8\times10^{11}\,\mathrm{s}^{-1}$ using axial magnetic field and $k_\perp/k_\parallel$ to be ±17 using the dispersion relation of lower hybrid waves. Here the sign of $k_\perp/k_\parallel$ depends on the direction in which lower hybrid waves propagate. Different signs of $k_\perp/k_\parallel$ correspond to different directions of the driving force. In LHCD experiments, the sign of $k_\perp/k_\parallel$ can be positive or negative, as a result toroidal rotations in both co-current and counter-current directions are predicted. Substituting these parameters into Eq. (72), we have the resonant-electron flow across flux surfaces $q_en_{er}u_{er}^r \sim \pm0.25\,\mathrm{A/m}^2$, where the sign is determined by that of $k_\perp/k_\parallel$.

With all the input quantities in Eqs. (25) and (26) determined, we can numerically solve the two equations for ion toroidal rotation. We apply a finite difference method in which the grid size is 1/400 of the minor radius a and the time-step is 1/200 of the thermal collision time $1/\nu_{enr,i}$. The numerical results are presented in Fig. 2. Shown in Fig. 2(a) is radial profile of toroidal velocity of ions for the case of $q_en_{er}u_{er}^r = -0.25\,\mathrm{A/m}^2$. The profile is plotted from plasma

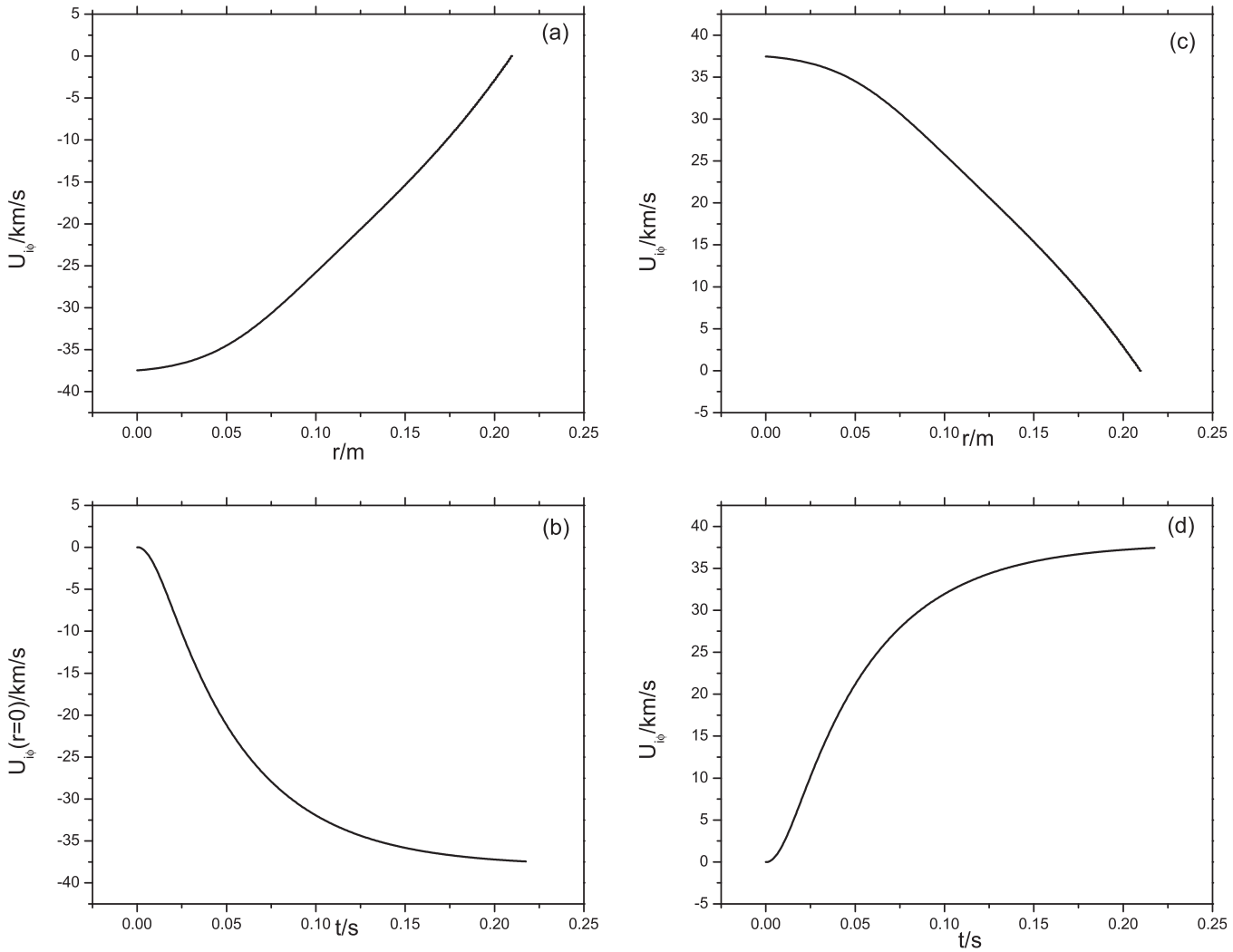

FIG. 2. (a) Radial profile of rotation speed with $q_e n_{er} u^r_{er} = -0.25\,\mathrm{A/m^2}$. (b) Time history of the rotation speed at plasma core for the same case as (a). (c) Radial profile of rotation speed with $q_e n_{er} u^r_{er} = 0.25\,\mathrm{A/m^2}$. (d) Time history of the rotation speed at plasma core for the same case as (c).

core $(r = 0\ \mathrm{m})$ to plasma edge at $r = a = 0.21$ m. The maximum rotation speed is –37 km/s, located at plasma core. Fig. 2(b) is the time history of the rotation speed at plasma core for the same case. Plotted in Fig. 2(c) is the radial profile of the rotation speed by taking $q_e n_{er} u^r_{er} = 0.25\,\mathrm{A/m^2}$. The peak speed is 37 km/s, which is also located at plasma core. The time history of the core rotation for this case is shown in Fig. 2(d). The symmetry with respect to the sign of u^φ_{enr}, u^φ_i, and u^r_{er} discussed at the end of Sec. II is evident from the numerical results shown in Fig. 2.

As displayed in Figs. 2(a) and 2(c), the rotation speed reaches its peak value at plasma core, this is consistent with experimental results.[17,18] The magnitude of the peak velocity shown in the above example is 37 km/s. The magnitude is determined by the driving force and momentum dissipation. A weaker momentum diffusivity, stronger return current or higher poloidal magnetic field can induce a stronger rotation. For the rotations in Alcator C-Mod, the peak velocity ranges from 20 km/s to 60 km/s.[17,18] Therefore, our model indeed predicts strong rotations comparable to experimental observations. The radial profile of rotation velocity is affected by the radial profile of return current, momentum diffusivity, momentum pinch-velocity, density, poloidal magnetic field, and other quantities. It is understandable that the profile of rotation shown above is different from the hollow rotation profile in the experiments.[17,18] The time scale of rotation is also important. The time history of flow in Figs. 2(c) and 2(d) can be fitted by exponential functions with a characteristic time of 65 ms, which is shorter than the typical 150 ms observed in experiments.[17] The reason of this difference might be that we have ignored the time it takes to establish toroidal current in Eq. (72). The driving force of rotation is proportional to the resonant-electron flow across flux surfaces which itself is proportional to the toroidal current as shown in Eq. (72). In practise, increase of the toroidal current will not be instantaneous because of the plasma internal inductance, neither will be the driving force. Therefore, we might be able to obtain results with more accurate characteristic time if we allow the toroidal current to have a finite increasing time. In experiment, normalized internal inductance is closely correlated with rotation speed. Although our model does not include the evolving of the inductance, it does indicate the existence of the correlation. The driving force of the rotation is proportional to wave-driving plasma current, and the normalized internal inductance

is just a measure of the radial profile of the current density. One significant advantage of our theory is that both counter-current and co-current rotations are predicted with different signs of $k_\perp/k_\parallel$ as shown in Fig. 2. Recent studies have reported that there are indeed toroidal rotations in both directions during launch of lower hybrid waves depending on specific experimental setups.[19,20] For example, the rotation speed is observed to increase by 30 km/s in the counter-current direction after the launch of lower hybrid waves for an initial toroidal current of 700 kA.[19,20] By lowering the initial toroidal current to 300 kA, the rotation speed increases by 20 km/s in the co-current direction after the launch of lower hybrid waves.[19,20]

V. CONCLUSION AND DISCUSSION

In this paper, we have presented a theoretical model to explain plasma rotations induced by lower hybrid waves observed in Alcator C-Mod. The driving force of the rotations is the Lorentz force on the bulk-electron flow across flux surfaces, which is a response of the plasma to the resonant-electron flow across flux surfaces induced by the lower hybrid waves. The flow across flux surfaces of the resonant-electrons and the bulk electrons are coupled through the radial electric field initiated by the resonant electrons, and the friction between ions and electrons transfers the toroidal momentum to ions from electrons. Toroidal rotations are determined using a set of fluid equations for bulk electrons and ions. However, the resonant-electron flow across flux surfaces cannot be found using the standard quasilinear theory[29,37] for velocity-space diffusion. We have developed an improved quasilinear theory to calculate the resonant-electron flow across flux surfaces as a result of velocity-space diffusion induced by lower hybrid waves. It turns out that it is necessary to include the gyrophase dependent part of the distribution function in the analysis. Velocity-space diffusion tensors for the zeroth and first gyrophase harmonics of the resonant-electron distribution function are derived, and kinetic equations for the first harmonics of the distribution function are solved. The resonant-electron flow is then calculated by taking the first moment of the first harmonics. A numerical code based on a finite-difference method is used to solve the fluid equations for the toroidal flow. The numerical results agree well with the experimental observation in terms of flow profile and amplitude.

In this theoretical model, the driving force of toroidal rotations is proportional to the toroidal current driven by the lower hybrid waves, as shown in Eq. (72). During the launch of lower hybrid waves, increasing the wave-driven current while fixing the total current is accompanied by variations in current density profile, which is usually measured by normalized internal inductance. Therefore, our theory has explained the mechanism of the strong correlation between rotation speed and normalized internal inductance observed in experiments.[17] In addition, it is able to explain the recent experiments in which both counter- and co-current rotations are observed during the launch of lower hybrid waves with different initial currents. Both counter-current and co-current rotations are predicted by this model depending on the sign of $k_\perp$. Different discharge configurations in experiments might have changed $k_\perp$, and thus resulted in different rotation directions. The theoretical model developed is also applicable to toroidal rotations observed in certain other tokamak experiments, for example, in discharges with ICRF heating. From Eq. (58), the lower hybrid waves are not the only mode that is able to drive resonant-particles to flow across flux surfaces. For this reason, we can follow the same procedure to calculate the Lorentz force and toroidal rotations induced by ICRF waves. Results in this direction will be reported in future publications.

ACKNOWLEDGMENTS

This research was supported by the U.S. Department of Energy (AC02-76CH03073), ITER-China program (2010GB107001), and National Natural Science Foundation of China (NSFC-11075162).

[1]A. Bondeson and D. J. Ward, Phys. Rev. Lett. **72**, 2709 (1994).
[2]R. Betti and J. P. Freidberg, Phys. Rev. Lett. **74**, 2949 (1995).
[3]K. C. Shaing and E. C. Crume, Phys. Rev. Lett. **63**, 2369 (1989).
[4]T. S. Hahm and K. H. Burrell, Phys. Plasmas **2**, 1648 (1995).
[5]N. J. Fisch, Phys. Rev. Lett. **41**, 873 (1978).
[6]T. H. Stix, Phys. Rev. Lett. **15**, 878 (1965).
[7]Y. Takase and M. Porkolab, Phys. Fluids. **26**, 2992 (1983).
[8]Y. Takase, M. Porkolab, J. J. Schuss, R. L. Watterson, C. L. Fiore, R. E. Slusher, and C. M. Surko, Phys. Fluids **28**, 983 (1985).
[9]R. L. Watterson, Y. Takase, P. T. Bonoli, M. Porkolab, R. E. Slusher, and C. M. Surko, Phys. Fluids **28**, 2622 (1985).
[10]R. Cesario and A. Cardinali, Nucl. Fusion **29**, 1709 (1989).
[11]R. Cesario, L. Amicucci, A. Cardinali, C. Castaldo, M. Marinucci, L. Panaccione, F. Santini, O. Tudisco, M. L. Apicella, G. Calabro, C. Cianfarani, D. Frigione, A. Galli, G. Mazzitelli, C. Mazzotta, V. Pericoli, G. Schettini, A. A. Tuccillo, and the FTU Team, Nature Commun. **1**, Article No. 55 (2010).
[12]G. M. Wallace, A. E. Hubbard, P. T. Bonoli, I. C. Faust, R. W. Harvey, J. W. Hughes, B. L. LaBombard, O. Meneghini, R. R. Parker, A. E. Schmidt, S. Shiraiwa, A. P. Smirnov, D. G. Whyte, J. R. Wilson, J. C. Wright, S. J. Wukitch, and the Alcator C-Mod Team, Nucl. Fusion **51**, 083032 (2011).
[13]G. M. Wallace, R. R. Parker, P. T. Bonoli, A. E. Hubbard, J. W. Hughes, B. L. Labombard, O. Meneghini, A. E. Schmidt, S. Shiraiwa, D. G. Whyte, J. C. Wright, S. J. Wukitch, R. W. Harvey, A. P. Smirnov, and J. R. Wilson, Phys. Plasmas **17**, 082508 (2010).
[14]M. Goniche, L. Amicucci, Y. Baranov, V. Basiuk, G. Calabro, A. Cardinali, C. Castaldo, R. Cesario, J. Decker, D. Dodt, A. Ekedahl, L. Figini, J. Garcia, G. Giruzzi, J. Hillairet, G. T. Hoang, A. Hubbard, E. Joffrin, K. Kirov, X. Litaudon, J. Mailloux, T. Oosako, R. Parker, V. Pericoli Ridolfini, Y. Peysson, P. Platania, F. Rimini, P. K. Sharma, C. Sozzi, and G. Wallace, Plasma Phys. Controlled Fusion **52**, 124031 (2010).
[15]R. Cesario, A. Cardinali, C. Castaldo, F. Paoletti, and D. Mazon, Phys. Rev. Lett. **92**, 175002 (2004).
[16]R. Cesario, L. Amicucci, C. Castaldo, M. Kempenaars, S. Jachmich, J. Mailloux, O. Tudisco, A. Galli, A. Krivska, and JET-EFDA contributors, Plasma Phys. Controlled Fusion **53**, 085011 (2011).
[17]A. Ince-Cushman, J. E. Rice, M. Reinke, M. Greenwald, G. Wallace, R. Parker, C. Fiore, J. W. Hughes, P. Bonoli, S. Shiraiwa, A. Hubbard, S. Wolfe, I. H. Hutchinson, E. Marmar, M. Bitter, J. Wilson, and K. Hill, Phys. Rev. Lett. **102**, 035002 (2009).
[18]J. E. Rice, A. C. Ince-Cushman, P. T. Bonoli, M. J. Greenwald, J. W. Hughes, R. R. Parker, M. L. Reinke, G. M. Wallace, C. L. Fiore, R. S. Granetz, A. E. Hubbard, J. H. Irby, E. S. Marmar, S. Shiraiwa, S. M. Wolfe, S. J. Wukitch, M. Bitter, K. Hill, and J. R. Wilson, Nucl. Fusion **49**, 025004 (2009).
[19]Y. A. Podpaly, J. E. Rice, R. R. Parker, M. L. Reinke, S. Shiraiwa, L. Delgado-Aparicio, S. Scott, P. Ennever, C. Gao, J. Irby, J. P. Lee, O. Meneghini, R. Mumgaard, M. Porkolab, N. Tsujii, J. R. Walk, and G. Wallace, PSFC/JA-11-30 (2011).

[20]Y. A. Podpaly, J. E. Rice, R. R. Parker, M. L. Reinke, L. Delgado-Aparicio, S. Scott, P. Ennever, D. Ernst, J. Irby, O. Meneghini, C. Gao, J. P. Lee, R. Mumgaard, M. Porkolab, S. Shiraiwa, N. Tsujii, J. R. Walk, and G. Wallace, APS DPP Conf. (2011).
[21]R. R Parker, Y. Podpaly, J. Lee, M. L. Reinke, and J. E. Rice, AIP Conf. Proc. **1406**, 455 (2011).
[22]O. D. Gurcan, P. H. Diamond, T. S. Hahm, and R. Singh, Phys. Plasmas **14**, 042306 (2007).
[23]P. H. Diamond, C. J. McDevitt, O. D. Gurcan, T. S. Hahm, W. X. Wang, E. S. Yoon, I. Holod, Z. Lin, V. Naulin, and R. Singh, Nucl. Fusion **49**, 045002 (2009).
[24]J. S. deGrassie, R. J. Groebner, K. H. Burrell, R.J. Groebner, and W. M. Solomon, Nucl. Fusion **49**, 085020 (2009).
[25]S. Wang, Phys. Plasmas **18**, 102502 (2011).
[26]Z. Gao, N. J. Fisch, and H Qin, Phys. Plasmas **18**, 082507 (2011).
[27]J. E. Rice, M. Greenwald, I. H. Hutchinson, E. S. Marmar, Y. Takase, S. M. Wolfe, and F. Bombarda, Nucl. Fusion **38**, 75 (1998).
[28]L.-G. Eriksson, E. Righi, and K.-D. Zastrow, Plasma Phys. Controlled Fusion **39**, 27 (1997).
[29]D. G. Swanson, *Plasma Waves*, 2nd ed. (Institute of Physics Publishing, 2003).
[30]N. J. Fisch, Rev. Mod. Phys. **59**, 175 (1987).
[31]N. J. Fisch and C. F. F. Karney, Phys. Fluids **24**, 27 (1981).
[32]K. Ida, Plasma Phys. Controlled Fusion **40**, 1429 (1998).
[33]J. E. Rice, W. D. Lee, E. S. Marmar, N. P. Basse, P. T. Bonoli, M. J. Greenwald, A. E. Hubbard, J. W. Hughes, I. H. Hutchinson, A. Ince-Cushman, J. H. Irby, Y. Lin, D. Mossessian, J. A. Snipes, S. M. Wolfe, S. J. Wukitch, and K. Zhurovich, Phys. Plasmas **11**(5), 2427 (2004).
[34]J. R. Wilson, R. Parker, M. Bitter, P. T. Bonoli, C. Fiore, R. W. Harvey, K. Hill, A. E. Hubbard, J. W. Hughes, A. Ince-Cushman, C. Kessel, J. S. Ko, O. Meneghini, C. K. Phillips, M. Porkolab, J. Rice, A. E. Schmidt, S. Scott, S. Shiraiwa, E. Valeo, G. Wallace, J. C. Wright, and the Alcator C-Mod Team, Nucl. Fusion **49**, 115015 (2009).
[35]T. S. Hahm, P. H. Diamond, O. D. Gurcan, and G. Rewoldt, Phys. Plasmas **14**, 072302 (2007).
[36]T. S. Hahm, P. H. Diamond, O. D. Gurcan, and G. Rewoldt, Phys. Plasmas **15**, 055902 (2008).
[37]T. H. Stix, *Waves in Plasmas* (Springer-Verlag, New York, 1992).
[38]J. C. Wright, E. J. Valeo, C. K. Phillips, P. T. Bonoli, and M. Brambilla, Commun. Comput. Phys. **4**, 545 (2008).
[39]J. C. Wright, P. T. Bonoli, A. E. Schmidt, C. K. Phillips, E. J. Valeo, R. W. Harvey, and M. A. Brambilla, Phys. Plasmas **16**, 072502 (2009).
[40]J. E. Rice, in 4th IAEA TM on Theory of Plasma Instabilities, Invited talk I-12 (2009).
[41]A. G. Peeters, C. Angioni, and D. Strintzi, Phys. Rev. Lett. **98**, 265003 (2007).